JOURNAL OF GEOPHYSICAL RESEARCH, VOL. 100, NO. D9, PAGES 18,707–18,726, SEPTEMBER 20, 1995

Contribution to the atmospheric mineral aerosol load from land surface modification

Ina Tegen

Department of Applied Physics, Columbia University, New York

Inez Fung[1]

NASA Goddard Institute for Space Studies, New York

Abstract. An estimation of the contribution of mineral dust from disturbed soils (i.e., soils affected by human activity and/or climate variability) to the total atmospheric mineral aerosol load is presented. A three–dimensional atmospheric dust transport model was used to simulate the distribution of dust optical thickness in response to individual dust sources, which include natural soils known to have been affected by the Saharan/Sahelian boundary shift, cultivation, deforestation, and wind erosion. The distributions extracted from advanced very high resolution radiometer (AVHRR) optical thickness retrievals were used to constrain likely source combinations. The results indicate that observed features like the seasonal shift of maximum optical thickness caused by Saharan dust over the Atlantic ocean are best reproduced if disturbed sources contribute 30–50% of the total atmospheric dust loading.

1. Introduction

The magnitude of radiative forcing and climate impact of aerosols is still largely uncertain. For an improved understanding of these processes, sources and atmospheric distribution of the different aerosol species have to be quantified.

Mineral dust is an aerosol type with one of the highest atmospheric mass loadings on a global scale besides sea–salt aerosol. The global source strength of mineral aerosol is currently estimated to a value between 1000 and 5000 Mt yr^{-1} [c.g., *Schütz,* 1980; *Duce et al.,* 1991; *Andreae,* 1994], compared to several hundred Mt yr^{-1} for sulfate aerosol [e.g., *Andreae,* 1994]. Mineral dust is also a predominant feature in satellite observations of aerosol optical thickness [*Rao et al.,* 1988] where dust plumes from the North African deserts over the North Atlantic ocean and over the Arabian Sea can clearly be recognized. In those areas the retrieved dust optical thicknesses can reach values of 0.6 to 1. The radiative impact of desert dust can be expected to be significant in areas with high dust loadings.

The term "radiative forcing" is generally used to describe the impact of anthropogenic atmospheric components on the Earth's radiation budget. In estimates of the radiative impact of aerosol types, mineral dust is usually classified as "natural" aerosol together with sea salt and volcanic aerosol, in contrast to "anthropogenic" aerosol like sulfate and nitrate aerosol from industrial emissions and soot from biomass burning. [e.g., *Andreae,* 1994]. The classification of mineral dust as "natural aerosol" is misleading if "natural" is interpreted as "not influenced by human activity", because the production of atmospheric mineral dust without doubt increases in areas where the soil surface is disrupted by agricultural activities or new soil surfaces are exposed to wind erosion through deforestation and shifting desert boundaries. For example, in the United States the highest dust production occurs in the area known in the 1930s and 1950s as "dust bowl", an area where the soil was disrupted by cultivation. The relative contribution of each source type to the atmospheric dust load is unknown, as dust measurements do not give information about the source type. *Penner et al.* [1994] states that anthropogenic mineral aerosol exists due to desertification and deforestation, but gives no estimate about the order of magnitude of the anthropogenic contribution to the atmospheric dust load.

The assumption that the non-natural sources, which are located at the semi-arid desert fringes rather than in the deserts themselves, contribute a major part of the atmospheric dust load is supported by various observations. Satellite observations [*Rao et al.,* 1988], ship measurements [*McDonald,* 1938], and observations of dust concentrations in Barbados and French Guyana [*Prospero et al.,* 1981; *Prospero and Nees,* 1986] show that the location of the Saharan dust plume, which extends

[1]Also at School of Earth and Ocean Sciences, University of Victoria British Columbia, Canada.

Paper number 95JD02051.
0148-0227/95/95JD-02051$05.00

over the North Atlantic ocean and transports dust over far distances toward South America, is subject to a seasonal shift following the Innertropical Convergence Zone (ITCZ). In the northern hemisphere winter, this dust plume is located around 5°–15°N, that is, south of the Sahara, while in the northern hemisphere summer, it is located around 15-25°N. These observations imply that this dust seems to originate from the Sahel region rather from the Saharan desert. *Prospero and Nees* [1986] report a strong increase in Saharan dust concentrations measured at Barbados from the mid-1960s to the mid-1980s, which is well correlated with the rainfall deficit in the Sahel since the late 1960s [*Lamb et al.*, 1986], while many authors find that dust production is only weakly correlated with mean rainfall in the source regions [e.g., *Pye*, 1987]. This finding also indicates that the Sahel, which is in contrast to the Saharan desert affected by cultivation, deforestation and overgrazing [*Middelton*, 1992; *World Resources Institute*, 1992], contributes significantly to the atmospheric dust load. Furthermore, Australia does not seem to export mineral dust into the Pacific ocean in a comparable order of magnitude as the North African deserts to the Atlantic Ocean, although the main vegetation types of Australia are desert and shrub land [*Matthews*, 1983].

In a transport model of mineral dust [*Tegen and Fung*, 1994], where only natural mineral dust sources were considered, the seasonal shift of the Saharan dust plume could not be reproduced, and the export of mineral dust from Australia was by far overestimated. This supports further the hypothesis that the atmospheric dust load cannot be explained by natural sources alone.

To obtain an estimate about which part of the dust load is caused by wind deflation from undisturbed soil and and which part originates from source areas influenced by human activity, we derived dust distributions for several different possible source types with the transport model described by *Tegen and Fung* [1994].

2. Mineral Dust Model

The desert dust transport model is described in detail by *Tegen and Fung* [1994]. It uses four different particle size classes which were treated as separate tracers. Particle sizes were derived from the $1° \times 1°$ data set of soil types and particle sizes [*Zobler*, 1986; *Webb et al.*, 1991], where the fractions of three major size classes are given as percentages of total soil mass in each grid box. The size classes are sand (particle radius larger than 25-μm diameter), silt (particle radius between 1 and 25 μm), and clay (particles smaller than 1 μm).

We assumed dust mobilization to be possible when the soil matric potential is higher than 10^4 J/kg, using monthly mean soil water contents as derived by *Bouwman et al.* [1993].

Several empirical studies show that the amount of uplifted dust follows [*Gillette*, 1978],

$$q_a = C(u - u_{tr})u^2, \qquad (1)$$

where q_a is the dust flux from the surface, u is the surface wind speed, and u_{tr} is a threshold velocity. The threshold surface wind speed at 10-m height is taken to be $6.5\,\mathrm{m\,s^{-1}}$, corresponding to *Kalma et al.* [1988]. We assumed the dimensional factor C to be constant for all size classes. To resolve high-frequency events in space and time, we used European Centre for Medium Range Weather Forecasts (ECMWF) (Tropical Ocean–Global Atmosphere (TOGA) Analysis) wind products (10 m–surface winds) with a spatial resolution of $1.125° \times 1.125°$ and 6–hour time resolution. With this parameterization the seasonal variation of dust uplift is described by the seasonality of surface winds and soil wetness.

The dust transport in the atmosphere was calculated using the three–dimensional Goddard Institute for Space Studies (GISS) tracer model ($8° \times 10°$ horizontal resolution, nine vertical atmospheric layers) [e.g., *Prather et al.*, 1987; *Fung et al.*, 1983], where source and sink terms were included. The model transports tracers by wind fields and subgrid–scale mixing statistics extracted from the GISS general circulation model (GCM).

Dust is removed from the atmosphere by wet and dry deposition. Wet deposition is parameterized using a scavenging ratio (the ratio of aerosol mass per unit rain mass and aerosol mass per unit air mass) $Z = 700$ with high–frequency precipitation statistics applied to monthly mean climatological precipitation data [*Shea*, 1986]. Dry deposition was described by gravitational settling and turbulent mixing as in *Genthon* [1992].

From this calculated atmospheric dust distribution, optical thicknesses τ were derived, using $\tau = Q\pi\hat{r}^2 N$ and $M = \frac{4}{3}\pi\rho\hat{r}^3$, where N is the number of particles, ρ is the particle density, $\hat{r}$ is a representative particle size, and Q is a extinction geometry factor with $Q \approx 2$ for large particles [*Fouquart et al.*, 1987]. We calculated the optical thickness with "typical" particle sizes of $r = 4\,\mu$m for small silt, and $r = 0.6\,\mu$m for clay, assuming a lognormal clay particle size distribution and a minimum size of $0.5\,\mu$m for individually uplifted clay particles in the atmosphere. Because of increased adhesive and cohesive forces due to their increased surface area, smaller particles tend to agglomerate and stick to larger particles [*Gillette et al.*, 1974]. Therefore we assumed that particles smaller than $0.5\,\mu$m are not available for wind erosion.

3. Dust Source Types

Given sufficiently low soil moisture and high surface wind speed, dust production can originate from various sources. Dust deflation can occur in deserts or sparsely vegetated areas, in cultivated land outside of the growing season, or in areas where the soil surface is freshly exposed to wind erosion after the vegetation cover is removed. The source strength for dust production, as well as the size distribution of the dust uplifted, may vary for different source types.

In the following, we separate dust source areas into two main classes: "natural" and "disturbed". "Nat-

ural" sources are assumed to have been acting for a long time, like deserts, whereas "disturbed" sources are those influenced by human activity (like cultivated or deforested areas) or by climate variability (like the Saharan/Sahelian boundary shifts).

Dust flux from disturbed sources may be stronger than dust flux from natural sources for two main reasons: freshly exposed soil can contain more fine material like silt (which contributes the major part of mineral aerosol) than "aged" soil surfaces, where fine material is likely to have been blown out already. For example, stabilized sand dunes do not act as dust sources [*Pye*, 1987]. Also, in cultivated areas the soil surface is in general disrupted by agricultural practices, in which case a lower threshold surface wind speed is sufficient to start dust deflation compared to undisturbed soil surfaces [*Gillette*, 1978; *Gillette et al.*, 1980].

Because of the short lifetime of dust in the atmosphere, we further divided "disturbed" sources according to their age into "old" and "recent" sources. By old sources, we mean areas where erosion is reported in the last 50 years, while recent sources are areas where changes in soil surface conditions occurred during the last decade. "Old, disturbed" areas are further subdivided into two: those where erosion was, or was not, associated with cultivation. "Recent disturbed" areas are subdivided into three: those associated with the Saharan/Sahelian boundary shift, recently cultivated areas, and recently deforested areas (but where cultivation is not reported).

The above classification results in six different dust source types, which are described in detail below. All source data sets were calculated in $1° \times 1°$ resolution.

Natural Sources
- NS Deserts and sparsely vegetated soils;

Old Disturbed Sources
- OA cultivated eroded soils; and
- OE uncultivated eroded soils;

Recently Disturbed Sources
- RB Saharan/Sahelian boundary shift;
- RC recently cultivated areas; and
- RD recently deforested areas.

The source strength of each source type is expressed as the percentage of area of each $1° \times 1°$ grid box is given that may act as a source of mineral dust, given sufficient low soil moisture and high surface wind speed.

Natural sources (NS)

Desert, grassland, and shrub lands are assumed to be natural dust sources. To obtain the distribution of the natural source regions, the vegetation data of *Matthews* [1983] was used to exclude regions with tall vegetation (e.g., forests) as possible dust source regions. Lithosols, as extracted from the soil type data set of *Zobler* [1986], were also excluded as possible sources. This soil type is defined as consisting of hard rock with less than 10–cm soil cover, and occur in mountainous regions (e.g., Himalayas), where dust production is unlikely [*Littmann*, 1991].

The contemporary distribution was obtained by subtracting the percentage of cultivated area [*Matthews*, 1983] from each $1° \times 1°$ grid box designated as a likely natural source. In grid boxes where no cultivation is recorded, three cases were investigated: the fraction of soil area that can act as dust source was assumed to be 10% (NS1), 50% (NS2), and 100% for Asian sources and 50% for other continents (NS3). Satellite observations that were used for constraining the dust export from the arid regions give only information about aerosol optical thicknesses over the ocean, that is, dust export from North Africa and Australia. In Asia, large loess deposits exist that may act as stronger dust sources compared to the sandy soils of the Sahara, this difference might be underestimated by the soil texture data set [*Zobler*, 1986] which was used to describe the initial soil particle size distribution. Condition NS3 was chosen to take the possibility into account that Asian deserts might be more productive dust sources than the North African or Australian deserts.

Old disturbed sources

Middelton [1992] and *World Resources Institute* [1992] describe regions where the soil is degraded as a result of deforestation, overgrazing, agricultural activities and overexploitation of vegetation for domestic use. They also report the percentage of area on each continent where the topsoil is affected by wind erosion. From the maps given in *Middelton* [1992], we identified countries where deflation of topsoil is reported. The percentage of area per grid box affected by erosion was chosen in a way that for each continent, the sum of affected areas per grid box agrees with the total area per continent. The latitudes between 18° and 28°N of the African continent were not included for this dust source type, as no soil degradation due to human activities is reported in the Saharan desert. In this way we obtained "continental source strengths" of this source type with additional regional information. The eroded soil areas were subdivided into cultivated and uncultivated areas.

Cultivated eroded soils (OA). The fraction of cultivated land per $1° \times 1°$ grid box is given in *Matthews* [1983] as five classes of cultivation intensity. As the most recent information used to compile the cultivation intensity data set was dated in the 1970s, we assumed that the regions identified in this data set have been disturbed for over 20 years. The cultivated areas that are colocated with erosion according to *Middelton* [1992] and *World Resources Institute* [1992] were included in this dust source class.

No dust deflation is assumed to take place during the growing season, when the root systems are supposedly holding the soil in place. For an estimation of the time period when the soil in cultivated areas is bare, the normalized difference vegetation index (NDVI) was used. During photosynthesis, green leaves absorb incident solar radiation at visible wavelengths strongly, but absorb less than 10% radiation in the near infrared. Therefore the difference in radiances in these spectral regions can be used as a measure for density of green vegetation.

NDVI is defined as

$$\mathrm{NDVI} = \frac{C_{NIR} - C_{VIS}}{C_{NIR} + C_{VIS}} \quad (2)$$

where C_{VIS} and C_{NIR} are reflected radiances at visible and in the near infrared wavelengths. The NDVI usually ranges from < 0.02 for desert areas to > 0.5 for fully developed green canopies [*Fung et al.*, 1987]. The NDVI data were calculated using radiances measured by the advanced very high resolution radiometer (AVHRR) instrument on board the NOAA series of polar-orbiting satellites. The mean monthly NDVI values were calculated for the years 1983 to 1987.

A threshold of NDVI < 0.07 was chosen, above which the ground cover by vegetation was assumed to be dense enough to inhibit dust deflation. This value agrees with the NDVI value for the $200\,\mathrm{mm\,yr^{-1}}$ precipitation isoline given by *Tucker et al.* [1991]

Uncultivated eroded soils (OE). Uncultivated eroded soils are those areas where erosion, but no cultivation, is reported. In these areas, the erosion is likely caused by overgrazing. Because livestock is not explicitly reported in the cultivation data set [*Matthews*, 1983], we obtained the percentage of affected area per continent for this source type by subtracting the percentage of cultivated area (OA) from the total eroded area.

Recently Disturbed Sources

We assume that recent dust sources to be those with origin in the past 20 years.

Saharan/Sahelian boundary shift (RB). *Tucker et al.* [1991] describe the Saharan/Sahelian boundary shift between the years 1980 and 1990. They report an average shift of the $200\,\mathrm{mm\,yr^{-1}}$ precipitation isoline from about 16°N to 15°N during that time period. It is unclear whether the Saharan/Sahelian boundary shift is caused by human activity like overgrazing or a consequence of natural variability [*Tucker et al.*, 1991].

We assumed this area to be a potential dust source, where 100% of the areas in those 1°×1° grid boxes which lie within the affected area are assumed to be dust sources. In grid boxes where also erosion (OA and OE) is reported, the fraction of eroded soil per grid box is subtracted from this source type so that the source area can not exceed 100% of the grid box if both source types are considered.

As the area affected by the Saharan/Sahelian boundary shift is only 6% of the total area of the Sahara, no noticeable difference in dust distributions would be obtained by adding this area to the natural dust sources (NS), if the emission factors for the disturbed and natural sources were the same.

Recently cultivated areas (RC). Soil surface newly disrupted for cultivation may act as dust sources. The decadal increase in cultivated area (cropland and pastures) per country is given between the years 1979 and 1989 in *World Resources Institute* [1992], and is expressed, for our study, as the percentage of newly cultivated land per country between 1979 and 1989. In contrast to the "old" cultivated sources, not only cropland but also pasture was considered to be cultivated land in this case. The newly cultivated lands were assumed to be uniformly distributed in each country, excluding deserts as identified by *Matthews* [1983] and areas with population densities less than $1000/\mathrm{km}^2$.

Recently deforested areas (RD). Deforestation, occurring mostly as a result of population pressures, leaves freshly exposed soils that may act as dust sources. The decrease in the area covered by forest per country is given between the years 1979 and 1989 in *World Resources Institute* [1992]. As for RC, we obtained the percentage of deforested land area per country from the statistics in *World Resources Institute* [1992] for the years 1979–1989. Deforestation was assumed to take place in those areas described as forest or woodland by *Matthews* [1983] and where the population density is higher than $1000/\mathrm{km}^2$.

As the source types RC and RD are most likely not independent of each other, we combined them into one source type (RL) which describes land use change. We assumed that in countries where deforestation and increase in cultivated area were reported simultaneously during 1979 and 1989, the deforested area is completely converted into cultivated land. This may lead to an underestimation of the recent dust source area, but this error is probably smaller than the error that would be introduced by assuming these source types to be independent of each other.

Plate 1 summarizes the geographical distribution of the source types described above. The colors indicate the areas where the different dust source types are possible. In the case of the recent sources it is indicated whether deforestation or conversion into cultivated land is predominant in the respective country. No indication about source strengths is given in the map. Overlap of different disturbed sources occurs only in a few areas, such as the Southern United States, Sahel, and Near East where both erosion and recent land use change is reported (types 5 and 6 in the map). In those areas the source strengths of the different types were added, assuming that in those cases the different source types were independent. The error that is introduced by this combination of sources is likely to be small, because in general the percentage of areas affected by land use changes per grid box are about an order of magnitude smaller than the percentage of area affected by erosion.

Table 1 summarizes for each source type the area per continent that may act as a dust source when low soil moisture and high surface wind speed occur. With this parameterization of the different source types, 10–67% of area per continent may act as a natural dust

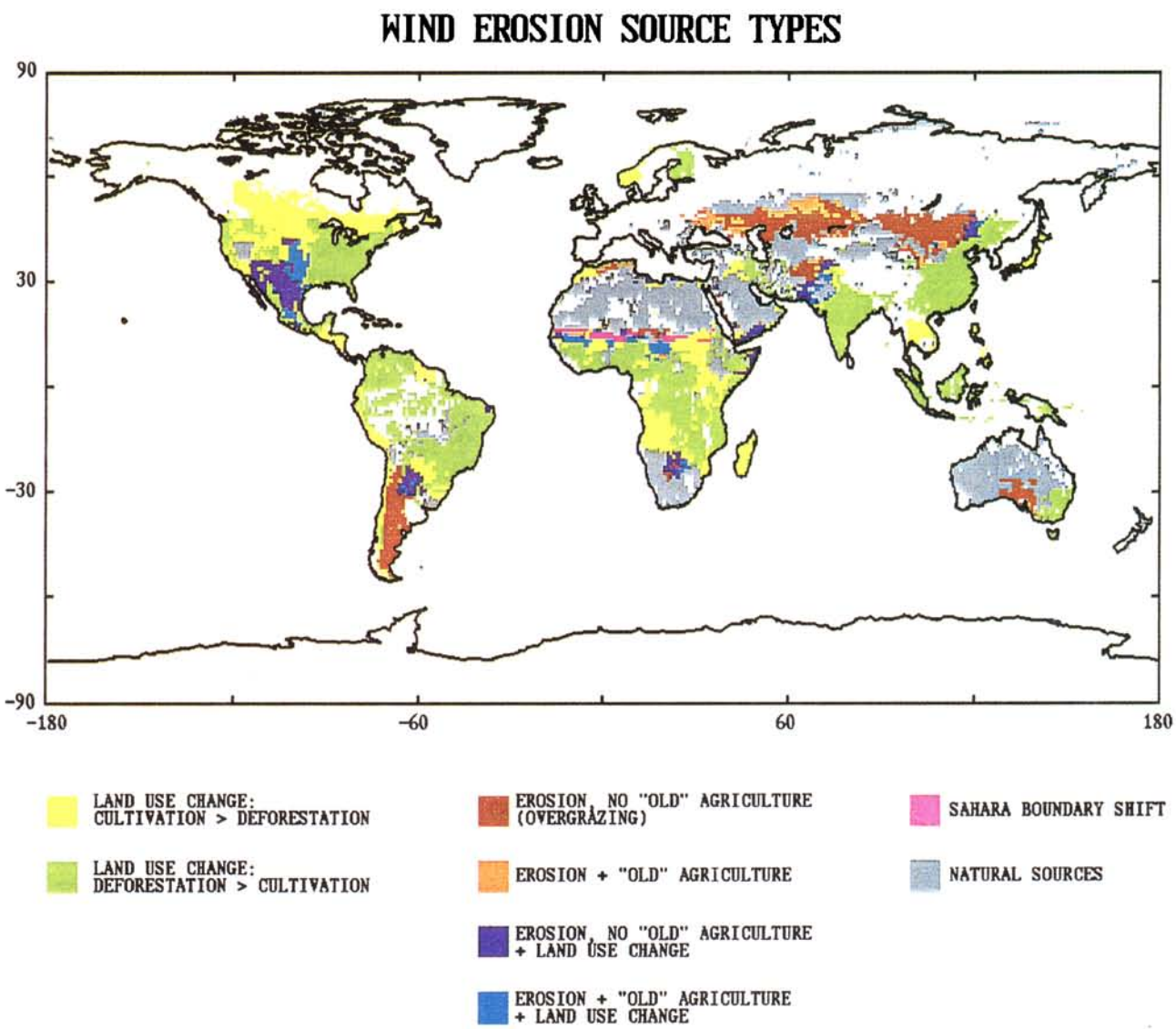

Plate 1. Geographical distribution of the different source types of mineral aerosol.

source, this source type is predominant with respect to the area. Old sources cover 0.4–4.1% of the continents, while recent sources cover 0.01 to 2.5 of the continaental area. These values are upper limits for areas that might act as dust source.

Figures 1a-1e show the annual mean optical thicknesses that are calculated with the transport model for each individual source type. The source strength of each source type was scaled with an annual global dust source strength of 3000 Mt yr^{-1} which is the "best guess" global estimate from *Tegen and Fung* [1994]. Figures 1a-1c all show relatively high dust optical thicknesses over the North Atlantic ocean west of the Sahara, over the Pacific ocean east of China, and over the Arabian Sea; these features show general agreement with satellite retrievals of optical thickness [*Rao et al.*, 1988].

4. Requirements for Contributions From Dust Source Types

Observed dust concentrations and optical thicknesses originate from several different source types. We attempted to combine the model results obtained from the individual source types in a way that calculated dust concentrations and optical thicknesses match observed features. This would yield an estimate of the contribution from disturbed sources to the atmospheric dust load.

There are only a few estimates of the production of mineral dust mass per continent [e.g., *Goudie*, 1983; *Duce et al.*, 1991], and most of them are derived from sedimentation rates into the ocean [e.g., *Sirokko and*

Table 1. Percentage of Land Area Per Continent That Can Potentially Act as Dust Source for Different Source Types

Source Type	Global	Africa	Asia	Europe	North America	South America	Oceania
Total Land Area (10^{10} m^2)	13014	2966	4256	951	2191	1768	882
NS Natural Sources (%)	34	54	26	10	18	38	67
OA Eroded Soil, cultivated (%)	1.2	1.3	2.0	4.1	0.6	0.4	0.5
OE Eroded Soil, not cultivated (%)	2.0	4.7	1.9	0.4	1.2	0.9	1.4
RB Sahara Boundary Shift (%)	0.4	1.6	0	0	0	0	0
RC Cultivated Area, recent (%)	0.5	0.3	0.2	0.007	0.7	2.2	0.003
RD Deforested Area (%)	0.5	0.5	0.4	0.005	0.2	2	0.05
RL Land use change (RC+RD)(%)	0.7	0.6	0.5	0.010	0.8	2.5	0.05

Sarntheim, 1989]. These estimations do not include dust deposited on land relatively close to the source areas. Another problem in the estimation of dust source strengths is the high variability of dust production in space and time. Therefore to obtain an estimate of the contribution of the various source types to the atmospheric mineral dust load, we compared regional seasonal variations resulting from different source distributions rather than total dust amounts.

We chose the following requirements that should be met by the calculated dust distribution.

1. A well-observed feature is the seasonal shift of the Saharan dust plume over the North Atlantic, following the ITCZ. The maximum dust concentration in the northern hemisphere summer is observed at 20°N and at 10°N in northern hemisphere winter. This seasonal shift is observed in ship measurements [*McDonald,* 1938], satellite observations [*Rao et al.,* 1988], and measurements of dust concentration at Barbados and French Guyana [*Prospero et al.,* 1981; *Prospero and Nees,* 1986]. Figure 2 shows a latitudinal cross section at 20°W of AVHRR optical thickness retrievals [*Ignatov et al.,* 1995; *Rao et al.,* 1988] for summer (JJA) and winter (DJF) 1990. A shift of the maximum optical thickness between 20°N in JJA and 9°N in DJF can be seen clearly. The usual explanation for this shift in the location of maximum dust concentration is the changing wind patterns by season [*Oort,* 1983]. Nevertheless, results from transport models of desert dust [*Joussaume,* 1990; *Wefers and Jaenicke,* 1990; *Tegen and Fung,* 1994], while showing a certain seasonal shift in the Saharan dust plume, all show maximum dust concentrations around 20°N rather than 10°N in the northern hemisphere winter, which is in disagreement with the observations.

A requirement for our modeled source distribution was chosen that the modeled dust concentration should reproduce this seasonal shift. It turns out that dust distribution from each source type reproduces the dust maximum at 20°N in northern hemisphere summer. Therefore the following requirement should be fulfilled by the modeled dust concentrations: The optical thickness over the North Atlantic Ocean west of the Sahara in the northern hemisphere winter should be lower at 20°N (τ_{20}) than at 10°N (τ_{10}). We calculated minimum amount of anthropogenic contribution to the atmospheric dust load that is necessary to meet the following requirements, respectively:

$$\delta = \frac{\tau_{10}-\tau_{20}}{0.5(\tau_{10}+\tau_{20})} > 0 \qquad \text{(Condition 1a)},$$

$$\delta = \frac{\tau_{10}-\tau_{20}}{0.5(\tau_{10}+\tau_{20})} > 0.7 \qquad \text{(Condition 1b)}.$$

The value of $\delta \approx 1$ of condition 1b is taken from the AVHRR optical thickness retrievals by *Rao et al.* [1988], allowing for an optical thickness of 0.06 due to biomass burning at 10°N. This value is estimated by using estimations for smoke emissions from burning of forests, savannahs, and grasslands by *Andreae* [1991], and calculating smoke distribution for 1 year with the GISS

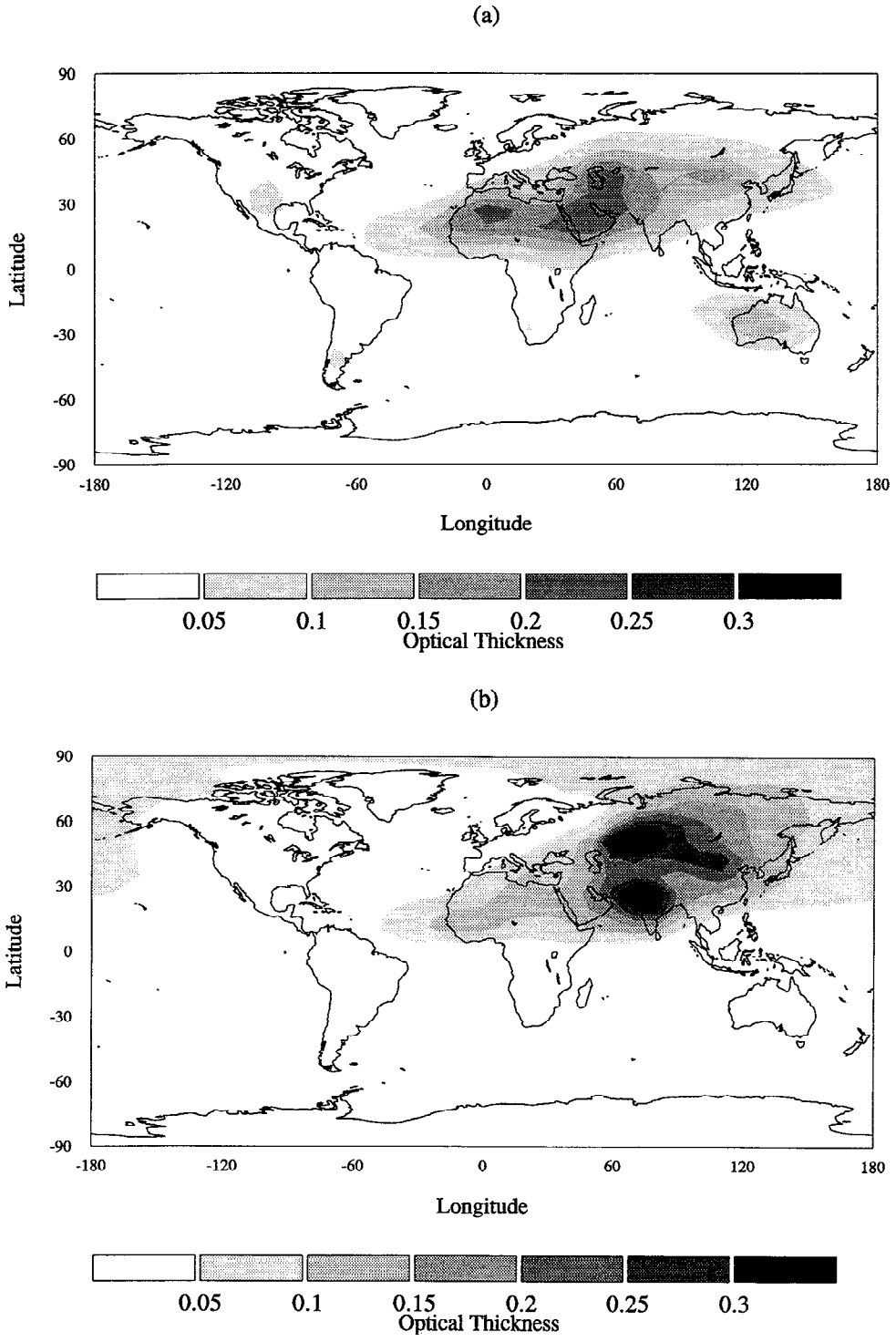

Figure 1. Annual mean optical thicknesses calculated with the transport model for each individual source type. (a) Natural sources (NS), (b) eroded, cultivated soil (OE) (c) eroded, uncultivated soil (OA) (d) land use change (deforestation, new cultivated areas) (RL) (e) Saharan Boundary shift (RB).

tracer model. Optical thicknesses of biomass burning smoke were calculated with the assumption of a particle density of $1\,g/cm^3$ and a mass-averaged radius of $0.3\,\mu m$ [*Penner et al.*, 1992].

2. Australia is probably not a strong source of desert dust compared to other arid regions. Maximum dust storm frequencies reported there are $15\,d\,yr^{-1}$, compared to 30-60 days $year^{-1}$ in various regions of Asia [*Pye*, 1987]. Optical thickness retrievals [*Rao et al.*, 1988] over the Pacific close to Australia usually do not exceed 0.1, compared with more than 0.4 at the location of the Saharan dust plume over the North Atlantic

(c)

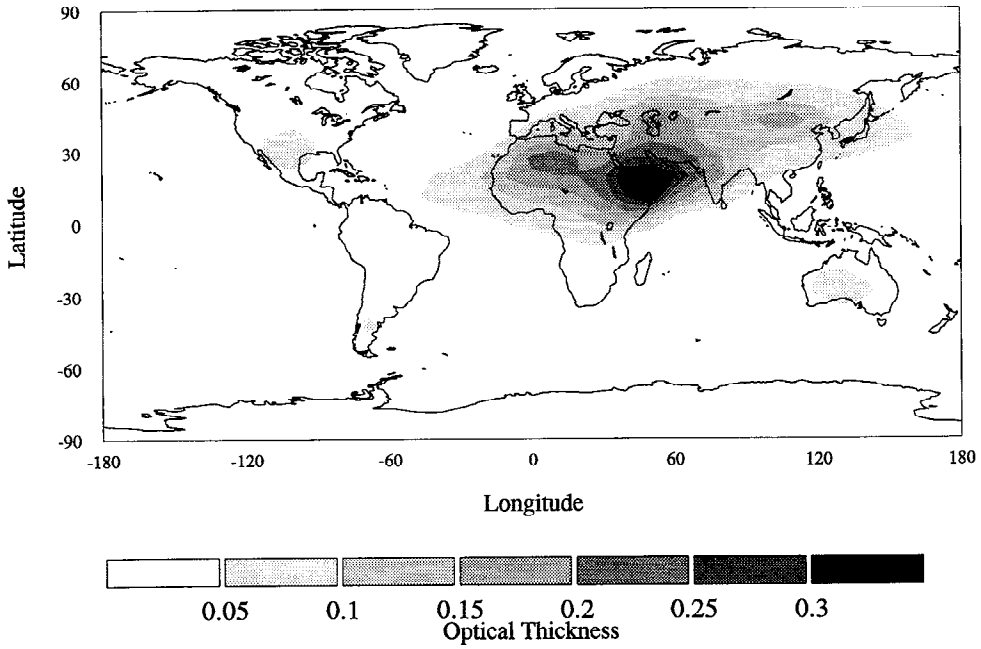

(d)

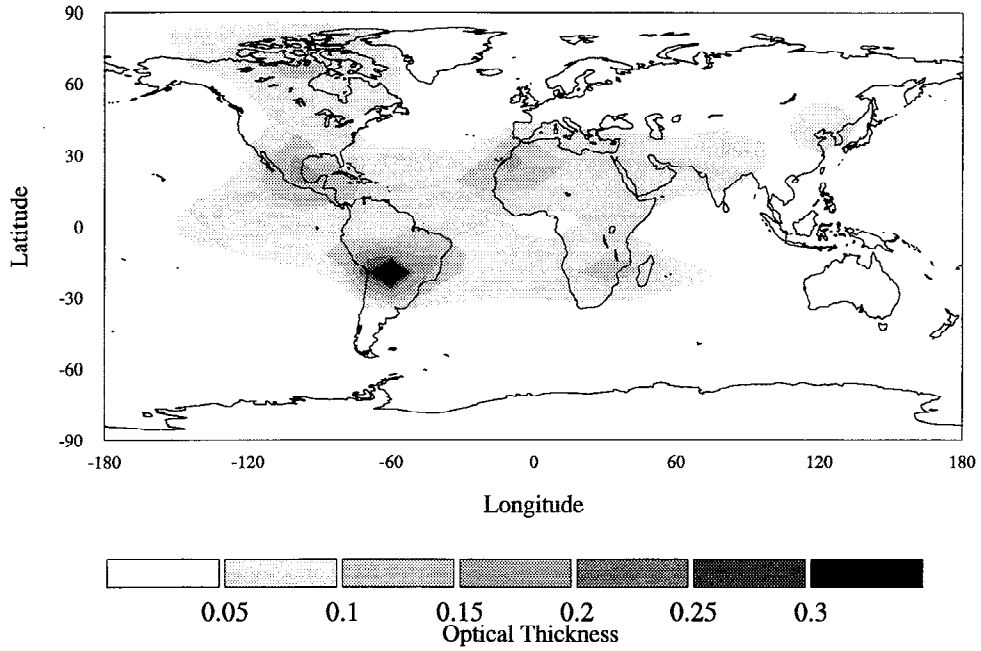

Figure 1. (continued)

or the maximum optical thickness over the Arabian sea in July and August of up to 0.6 and 1. As the absolute value of dust optical thickness retrieval from satellite data is uncertain, we applied the following requirement to the calculated dust optical thicknesses.

$$\rho = \tau_{ar}/\tau_{aus} > 3 \qquad \text{(Condition 2)},$$

where τ_{aus} is the maximum dust optical thickness over the South Pacific in the model grid boxes next to Australia, and τ_{ar} is the maximum dust optical thickness modeled over the Arabian Sea.

3. The seasonal variation of dust storm frequencies is well observed at several locations. Modeled seasonal variations of the mineral dust load should be in agreement with these observations. Observed seasonal variations in dust storm frequencies reported by *Littmann* [1991] in China (maximum: April), Sahel (maximum: February - April), India (maximum: June),

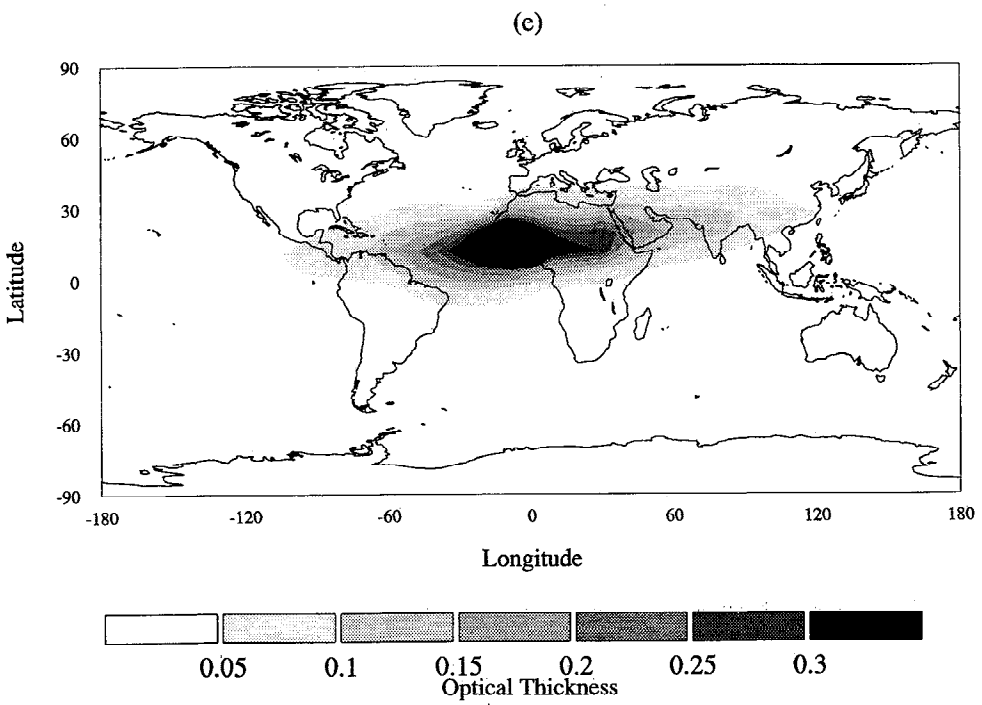

Figure 1. (continued)

and Middle East (maximum: July - August) were compared to the modeled seasonal variations of dust concentrations for the different source types at those locations.

For conditions 1a and 1b to be useful, we must first establish that the reasons for the model's failure to reproduce the seasonal shift in maximum optical thickness between 10° and 20°N in the Atlantic is caused by an unrealistic source distribution and not by an unrealistic wind field in the transport calculation. In Figures 3a and 3b the wind vectors of the first model layer for the northern hemisphere winter in the Sahara/Sahel region are compared with the corresponding wind vectors from observations [*Oort*, 1983]. Additionally shown is the isoline of the optical thickness of 0.3 from the AVHRR satellite retrieval of aerosol optical thickness.

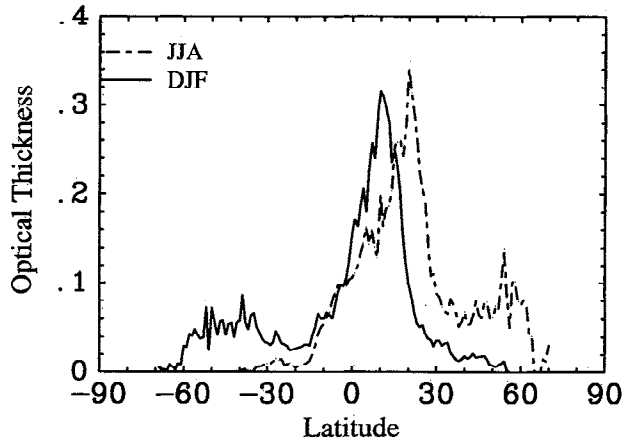

Figure 2. Latitudinal cross section at 20°W of AVHRR optical thickness retrievals for summer (JJA) and winter (DJF) 1990.

The model winds underestimate the north-south advection and overestimate the east-west advection over the Sahara. It might be possible that more realistic model winds would reproduce the seasonal shift of the Saharan dust plume for desert sources. On the other hand, the dust model of *Wefers and Jaenicke* [1990] which is based on monthly mean wind fields from *Oort* [1983] also shows a maximum in dust optical thickness at 20°N rather than at 10°N in winter for a desert source. Also, the location of the grid box we used to calculate δ is actually located between 8° and 16°N, slightly northward of the maximum optical thickness located between 6° and 12°N in the AVHRR retrieval. Taking the weaker north-south advection for the model winds into account, it can be argued that the air masses carrying maximum dust optical thickness have crossed approximately the same areas in the model as in the real world. Therefore we assume the conditions 1a and 1b can be used with our transport model. For the month of January, the dust transport has been calculated additionally with the new 4° × 5° version of the GISS GCM [*Druyan et al.*, 1994] where north/south advection of the model winds over North Africa is more realistic. The results of that experiment agreed with the results for the 8° × 10° tracer model winds. Nevertheless, this point has to be further addressed in the future, for example, by using more realistic model winds or validating the assumptions about the origin of the air masses by means of other tracers.

5. Experiments and Results

Table 2 summarizes results of the tracer model for the individual sources. It gives the areal extent of the

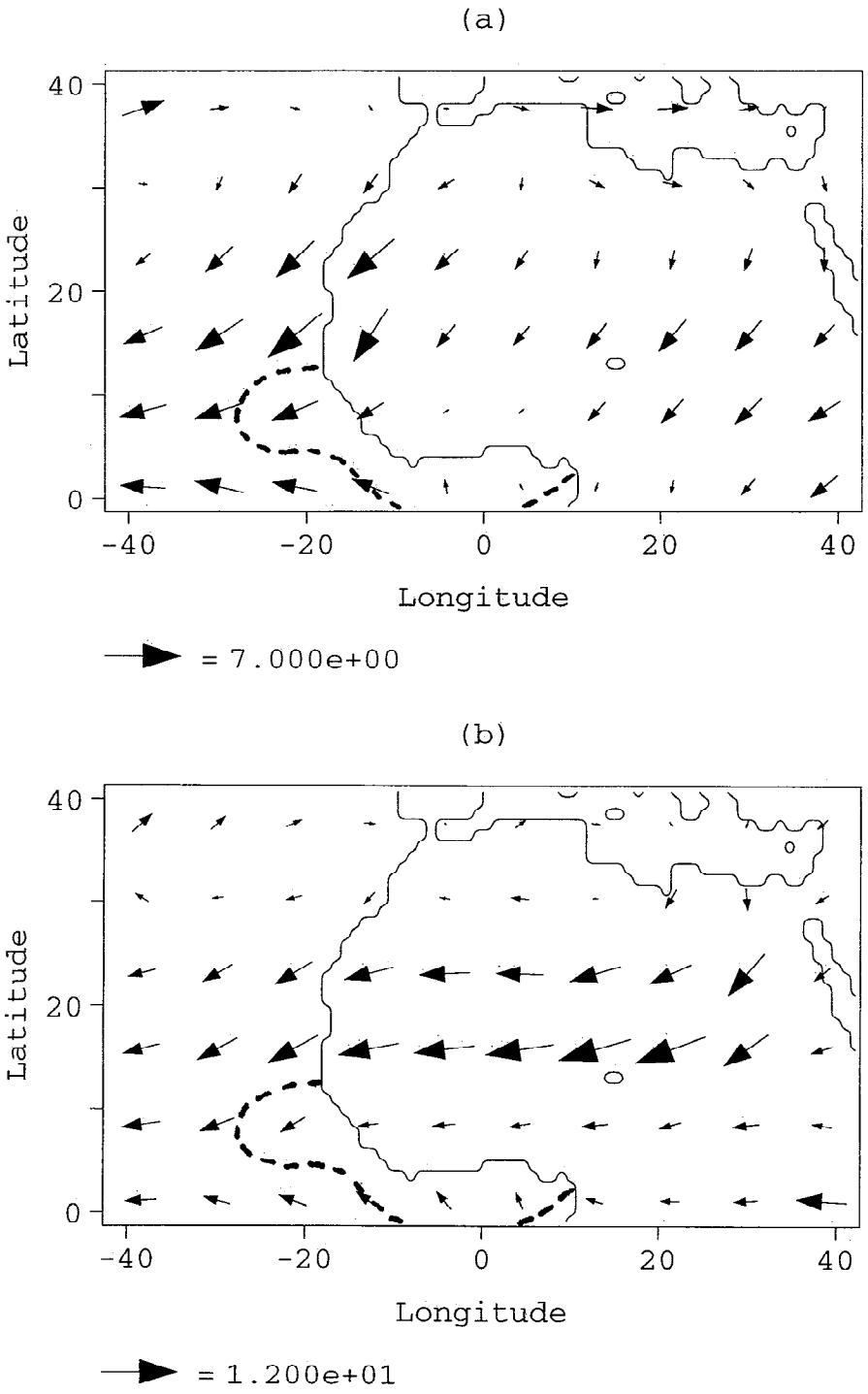

Figure 3. Wind vectors of the first model layer (a) for the northern hemisphere winter in the Sahara/Sahel region and corresponding wind vectors from observations [*Oort*, 1983] (b). The contour line describes the isoline of optical thickness of 0.3 from the AVHRR satellite retrieval of optical thickness.

sources in the model as well as the areas expressed as percentage of total land area. The difference between these percentages and the percentage values in Table 1 is that these values describe the fraction of the area where the surface wind speed is sufficiently high and the soil moisture is sufficiently low to allow dust deflation. For most source types about 10% of the global "potential" source area is an "active" source area in the model. In the case of "old" sources, about 20-25% of the "potential" source area is active. Including the Saharan/Sahelian boundary shift, the recent source areas are only about 20% of the old source areas.

The values for $\delta = \frac{\tau_{10}-\tau_{20}}{0.5(\tau_{10}+\tau_{20})}$ and $\rho = \tau_{ar}/\tau_{aus}$ are also given in Table 2 for the individual sources.

Table 2. Total Areas and Percentages of Global Land Area Ahat are Active Dust Sources in the Model (Sufficient High Wind Speed and Low Soil Moisture Occurs) and Dust Properties From These Sources

Source type	Area, 10^{10} m^2	Land Area, %	$\delta = \frac{\tau_{10}-\tau_{20}}{0.5(\tau_{10}+\tau_{20})}$	$\rho = \tau_{ar}/\tau_{aus}$
NS1, Natural Sources [1]	780	6	-0.28	1.9
NS2, Natural Sources [2]	390	3	-0.28	1.9
NS3, Natural Sources [3]	510	4	-0.2	2.9
OA, Eroded soil, cultivated	36	0.3	0.53	3.0
OE, Eroded soil, not cult.	44	0.4	0.05	7.0
RL, Land use change	9	0.07	0.17	1.6
RB, Sahara boundary shift	6	0.05	0.6	17.3

[1] 100% of area each grid box acts as source
[2] 50% of area each gridbox acts as source
[3] Asian deserts 100%, other deserts 50%

Condition 1a ($\delta > 0$) is not satisfied for the natural sources NS1–NS3, but for all disturbed source types ($0.05 < \delta < 0.53$). No source type alone fulfills condition 1b ($\delta > 0.7$). This may be due to incomplete representation of aerosols from biomass burning to the total aerosol optical thickness: we included the burning of forests, savannas, and grasslands and did not consider smoke from fuel wood burning due to lack of information. Therefore no mixture of natural and anthropogenic dust will fulfill condition 1b. Condition 2 ($\rho > 3$) cannot be fulfilled for source types RD (deforestation) or RL (land use change). These source types are unlikely to be the only dust sources. For the natural dust sources, ρ is 1.9–2.9, slightly below the observed value of > 3 for (condition 2). Thus natural sources alone cannot meet the required conditions 1a and 2. On the other hand, with exception of RD and RL, all anthropogenic sources fulfill those conditions.

We estimated the minimum contribution from disturbed dust sources to the global atmospheric dust load necessary to fulfill the conditions 1a and 2 for nine scenarios that are summarized in Table 3. As we are considering the seasonal and regional variation in dust distributions rather than the total dust mass, the source strengths of experiments were scaled to a total global dust source strength of 3000 Mt/yr for the sum of all source types.

Experiments 1–3 are combinations of natural sources NS2 (50% of the area is possible dust source) and "old" sources OA and OE. Experiments 4-6 are combinations of NS2 and "recent" sources RD, RL, and RB. Experiments 7-9 are combinations of natural with old and recent sources. In experiment 7 (combination C1) the disturbed sources include cultivated (OA) and uncultivated eroded soil (OE) and land use change (RL), but not the Saharan/Sahelian boundary shift. In experiment 8 (C2) the disturbed soils include also the Saharan/Sahelian boundary shift (RB). Experiment 9 (C3) is a combination of disturbed sources corresponding to experiment 8 and natural sources NS3 (Asian deserts being twice as productive as deserts from other continents)

In the experiments with more than one disturbed source type, these sources were assumed to have an identical emission factor (1) for each source type (i.e., 1-m^2 of cultivated area produces the same amount of dust as 1-m^2 deforested area at the same wind speed). The total source strengths (disturbed plus undisturbed sources) are scaled to a total annual emission of 3000 Mt dust.

Figures 4a–4c show the dependency of the ratio $\delta = \frac{\tau_{10}-\tau_{20}}{0.5(\tau_{10}+\tau_{20})}$ on the percentage of dust mass from disturbed sources for each experiment, respectively. From these curves the necessary minimum contribution from disturbed sources to fulfill condition 1a ($\delta > 0$) can be obtained. These results are summarized in Table 3. The minimum disturbance contribution to fulfill condition 1a lies between 8 and 88%. The condition 1b ($\delta > 0.7$) cannot be fulfilled for any source combination.

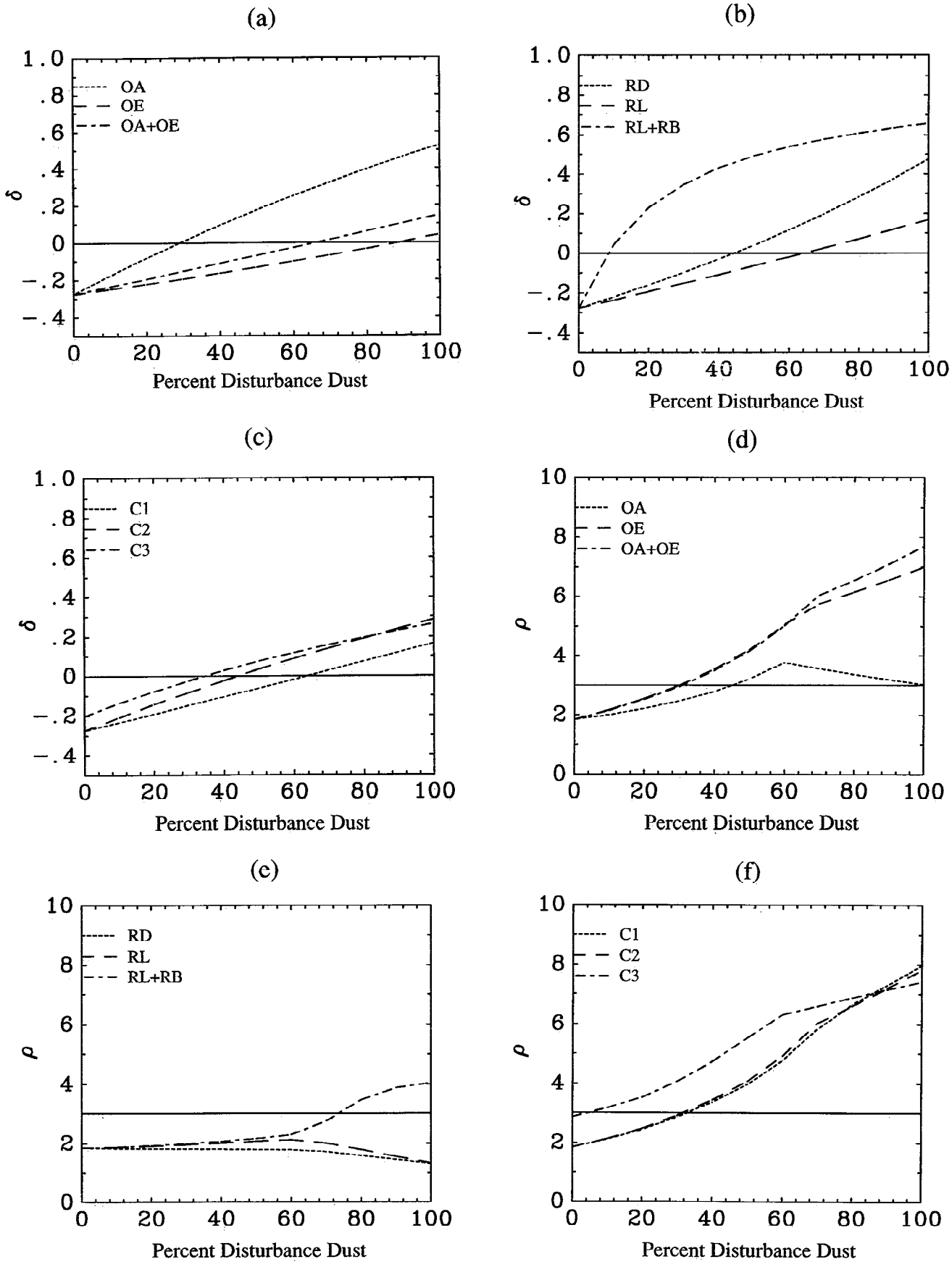

Figure 4. (a)–(c) Dependency of the ratio $\delta = \frac{\tau_{10}-\tau_{20}}{0.5(\tau_{10}+\tau_{20})}$ on the percentage of dust mass from disturbed sources for each experiment. (d)–(e) Dependency of $\rho = \tau_{ar}/\tau_{aus}$ on the percentage of dust mass from disturbed sources for each experiment.

Table 3. Minimum Percentage of Anthropogenic Dust Per Source Type, Depending on Conditions 1a ($\delta > 0$) and 2 ($\rho > 3$) and Emission Factors for the Case of 50% Disturbance Contribution to Total Atmospheric Dust Mass, 3000 Mt yr^{-1}

Experiment	Source Types	Condition 1a*	Condition 2*	Emission Factor $\mu g\,s^2\,m^{-5}$	Emission Factor $\mu g\,s^2\,m^{-5}$
1	NS2, OA	> 30%	> 46%	0.6	19.3
2	NS2, OE	> 88%	> 30%	0.6	3.0
3	NS2, OA, OE	> 66%	> 30%	0.6	2.6
4	NS2, RD	> 43%	–	0.6	179
5	NS2, RL	> 64%	–	0.6	82
6	NS2, RL, RB	> 8%	> 73%	0.6	43
7	NS2, OA, OE, RL	> 64%	> 5%	0.6	2.5
8	NS2, OA, OE, RL, RB	> 44%	> 32%	0.6	2.4
9	NS3, OA, OE, RL, RB	> 34%	> 33%	0.83	2.4

*The minimum contribution for disturbance sources to fulfill condition 1a and 2.

To fulfill condition 2 ($\rho > 3$) (Figures 4d–4e) at least 5-73% has to originate from disturbed sources (Table 3). In the case of experiments 3 and 4, the maximum value for ρ is below 3, therefore condition 2 cannot be fulfilled for these experiments. For the experiment where we assumed Asian deserts to be twice as strong dust sources than deserts from other continents (experiment 9), the required minimum contribution of disturbed dust mass is 33% to meet both conditions 1a and 2; for all other source type the minimum contribution is more than 40%. Although the results for the different sources differ widely, they indicate that at least 30% of the atmospheric dust load should originate from disturbed sources with the chosen source type parameterization.

For the same global emission, the dimensional "emission factor" C from (1) would be different for each source type, as each source type has different areal coverage. Table 3 shows the emission factors for experiments 1–9 for a contribution of 50% from disturbed sources to the atmospheric dust load, that is, the natural and the sum of disturbed sources each have a global source strength of 1500 Mt yr^{-1}. From measurements reported by *Gillette* [1978] and *Jaenicke* [1988], emission factors of about 0.5–2 $\mu g\,s^2\,m^{-5}$ for undisturbed soils can be deduced. For a 50% contribution from disturbed to the total dust load, the value of 0.6 $\mu g\,s^2\,m^{-5}$ for NS2 (50% of area act as dust source) appears to be realistic. (If 100% of the undisturbed source areas were a potential dust source (NS1), this the emission factor would be 0.3 $\mu g\,s^2\,m^{-5}$, which is probably too low). The emission factors thus obtained for disturbed sources are higher than the natural sources by factors of 4–300. This agrees with the results of *Gillette* [1978], who observed in wind tunnel experiments that the amount of deflated dust is about 1 order of magnitude higher for disturbed soils than for undisturbed soils. The high values of the emission factor for the recent sources (experiments 4–6) of 43–179 $\mu g\,s^2\,m^{-5}$ would certainly be upper limits, as it is highly unlikely that these sources are the only disturbed source types.

Consideration of the emission factor leads to an additional constraint on the estimate of the disturbance contribution to the dust load. *Westphal* [1987] states that only 10% of the Sahara is a potential dust source. If this condition is applied globally for all natural sources, emission factors between 0.5 and 2 $\mu g\,s^2\,m^{-5}$ would result for global source strengths between 300 and 1000 Mt yr^{-1}. Assuming a total global source strength of 3000 Mt yr^{-1}, 2000–2700 Mt dust per year would have to originate from disturbed soil. These calculations suggest that 60–90% of the atmospheric dust load would have to originate from other sources, that is, disturbed soils.

The seasonal variations of modeled dust concentration are shown in Figures 5a-5d at the locations China, India, Middle East (Iran), and Sahel, compared to observed seasonal variations reported by *Littmann* [1991]. All source types reproduce the observed seasonal variation reasonably well. This shows that at these sites

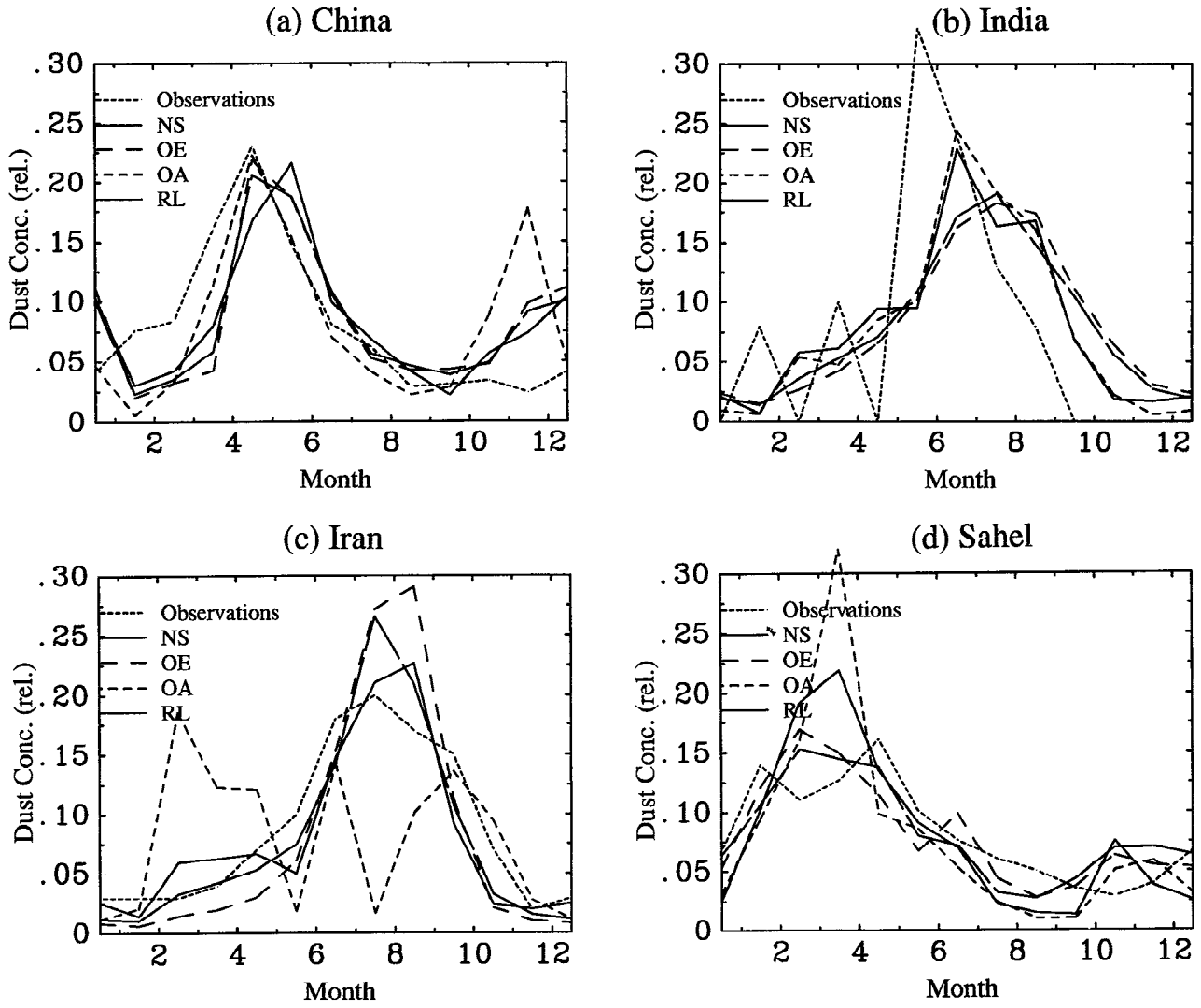

Figure 5: Seasonal variations of modeled dust concentration at the locations (a) China, (b) India, (c) Middle East (Iran), and (d) Sahel, compared to observed seasonal variations reported by *Littmann* [1991] in relative units.

seasonal variations in dust concentration are caused by changing patterns of surface wind speed and soil moisture rather than by the difference in the geographic distribution of the various source types. The seasonal variation at those sites therefore cannot be used as an additional constraint on the contributions from individual source types.

Plate 2a and 2b shows the resulting modeled dust source strengths for the case of 50% contribution to the dust load from natural soils and disturbed soils (combined sources, experiment 8), respectively. The global annual dust emission for each of both source types is set to to $1500\,\mathrm{Mt\,yr^{-1}}$. The modeled major dust source areas in North America, Asia, and Australia are in good agreement with areas of high dust storm activities reported by for example, *Pye* [1987]. For the United States, the areas of modeled maximum dust emission from disturbed soils (parts of Oklahoma, Texas and Kansas) agree with areas of maximum dust production between 100° and 105°W reported by [*Gillette and Hanson*, 1989]. *Gillette and Sinclair* [1990] find that about 60% of the dust emission in the United States is caused by local convective circulations (dust devils). They estimate a dust flux of about $6\,\mathrm{g/(m^2\,yr)}$ for particles smaller than 25 μm caused by dust devils. This is in agreement with the modeled dust flux from natural sources, which is about $10\,\mathrm{g/(m^2\,yr)}$ in North America (only particles smaller than 50 μm were considered in the dust transport model).

Figures 6a and 6b show the seasonal variation of modeled dust optical thicknesses for the case of 50% contribution from disturbed soils to the total dust load for the experiment 8 (best guess), compared to the seasonal variations for only natural sources NS (Figure 6c and 6d). As in all experiments with dust contribution from disturbed soils, the seasonal shift of the Saharan dust plume following the ITCZ is better reproduced for the best guess case compared to the case of only natural dust. All experiments reproduce the maximum in dust optical thickness over the Arabian sea during northern hemisphere summer.

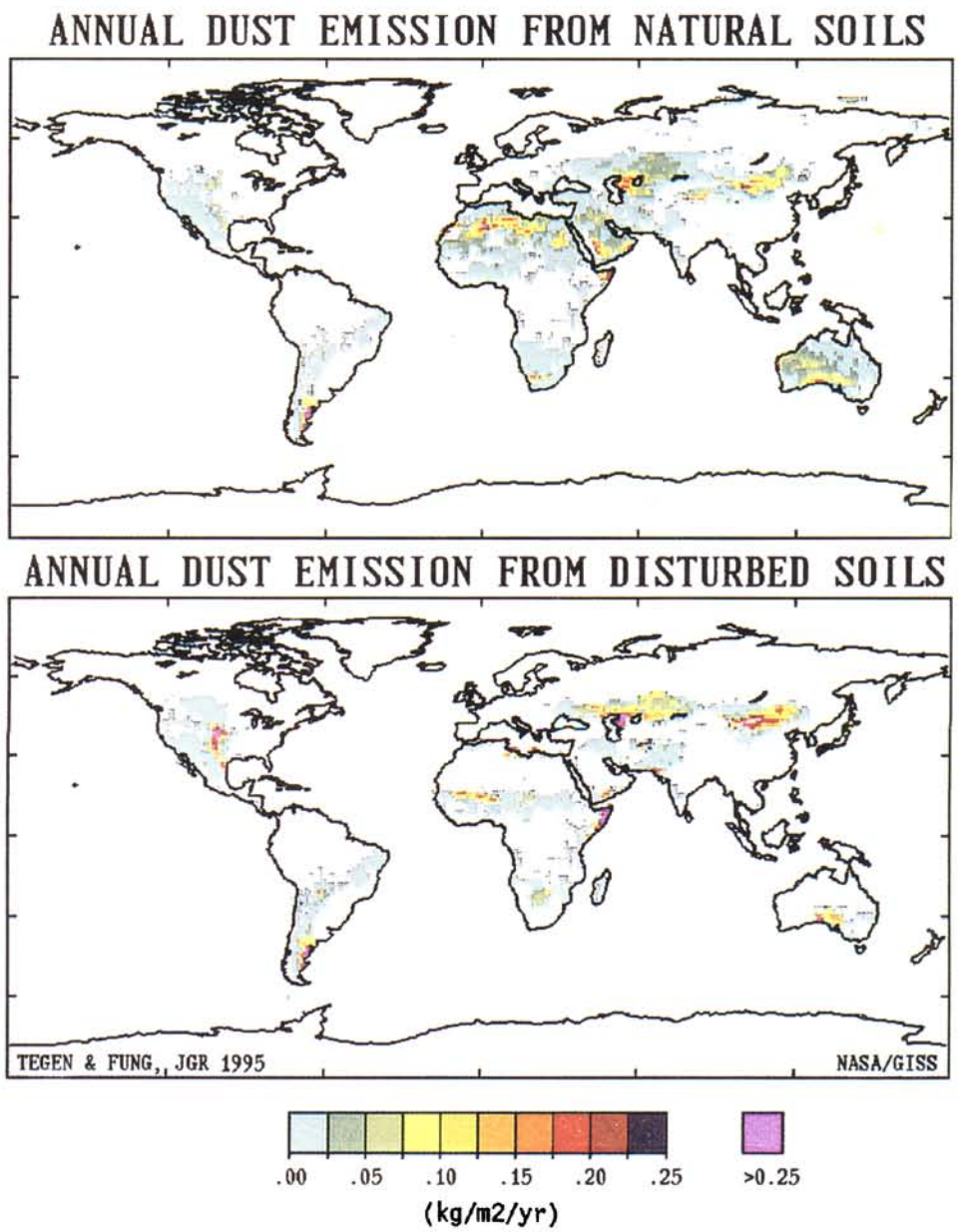

Plate 2. Modeled annual dust emission from (a) natural and (b) disturbed soils for the case of 50% contribution from disturbed soils to the total dust load. The global annual dust emission for each of both source types is 1500 Mt yr^{-1}.

Figure 7 compares the difference in optical thickness between winter and summer month at a latitude of 20°W, as estimated from the AVHRR data product, the model results for only natural sources, and the best guess result (experiment 8 with 50% contribution of dust from disturbed sources). Obviously, the seasonal shift of the Saharan/Sahelian dust plume is better reproduced for the case of 50% dust from disturbed sources.

For the best guess case, we calculated not only the ratio (ρ) of dust optical thickness over Saudi Arabia to that over Australia, but also the ratios of optical thickness at several other locations over the ocean to the optical thickness at Australia during northern hemisphere winter. The locations chosen were regions where the optical thickness can be expected to be strongly influenced by dust aerosol: (30°N, 30°W), (20°N, 30°W), (10°N, 60°E), and (10°S, 5°E) in northern hemisphere summer, (40°N, 150°E) in northern hemisphere spring, and (10°N, 30°W) in northern hemisphere winter. The comparison of the modeled optical thickness ratios with the AVHRR optical thickness ratios is shown in Figure 8 for the best guess case and for only natural sources. If the optical thickness ratios for the best guess model case are corrected for biomass burning optical thickness, the results are almost linear with the AVHRR optical thickness ratios. In the case of the model results for only natural sources, the ratios are generally smaller than the observations, as the dust optical thickness over Australia is relatively high for this case. Also they are not linear with the AVHRR optical thickness ratios. This supports further the assumption of a con-

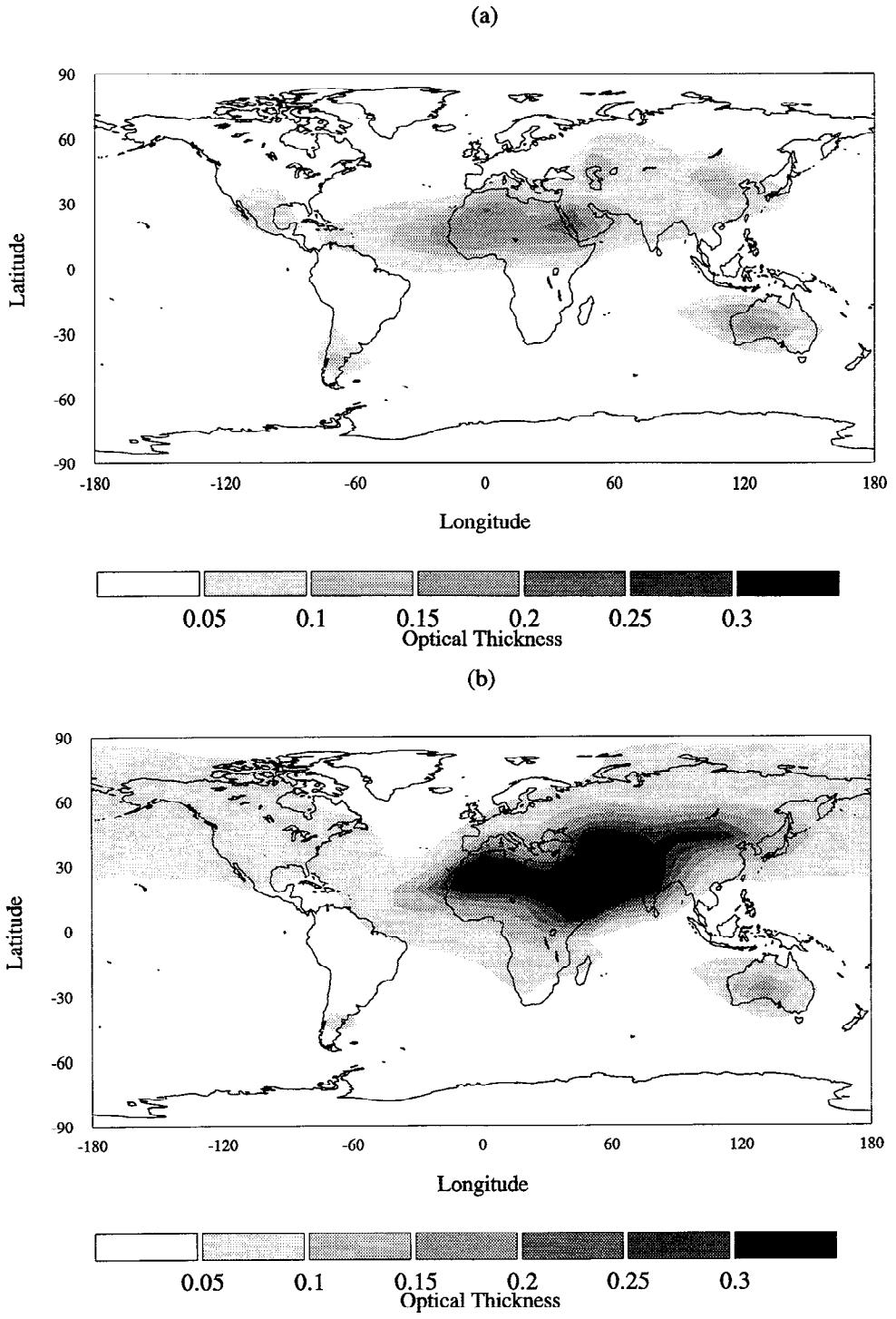

Figure 6. Modeled dust optical thicknesses for the case of 50% contribution from disturbed soils to the dust load for the experiment 8 (best guess) for (a) December–February and (b) June–August, and seasonal variations for only natural sources NS for (c) December–February and (d) June–August.

siderable contribution from dust from disturbed sources to the atmospheric dust load.

Figures 9a and 9b show the annual mean optical thickness for the best guess case in comparison with the annual mean of the AVHRR optical thickness data product (for the year 1990). The comparison shows that the calculated optical thickness correspond well to the optical thickness retrievals over the ocean, but also emphazises the need of satellite measurements of aerosols over land. Although few attempts of satellite optical thickness retrievals of dust over land have been made [e.g., *Fraser*, 1993], these are limited to well-known dust events and are only possible over dark surfaces.

(c)

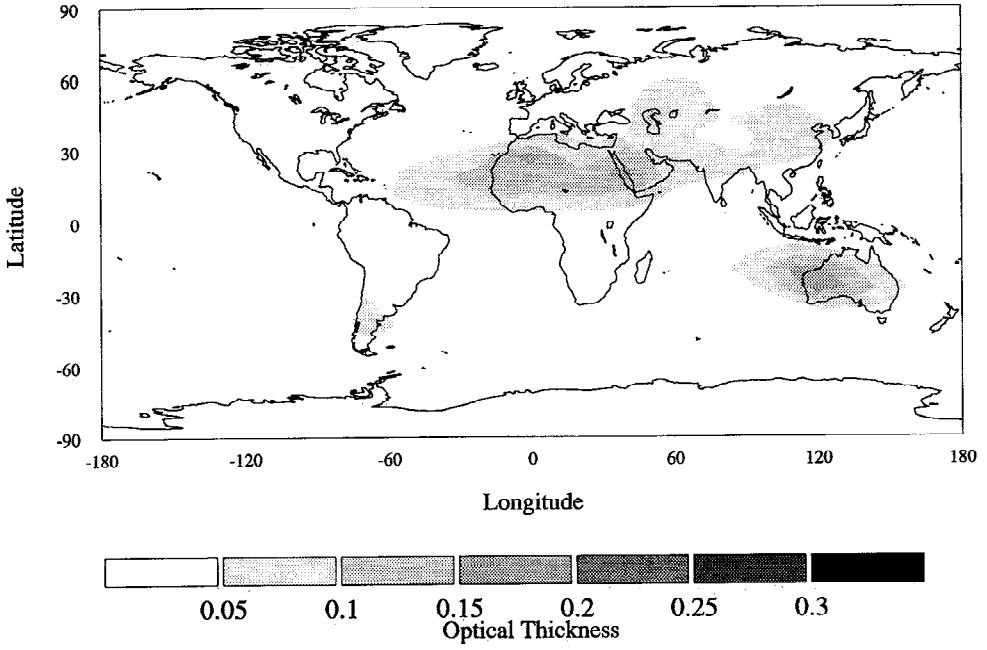

(d)

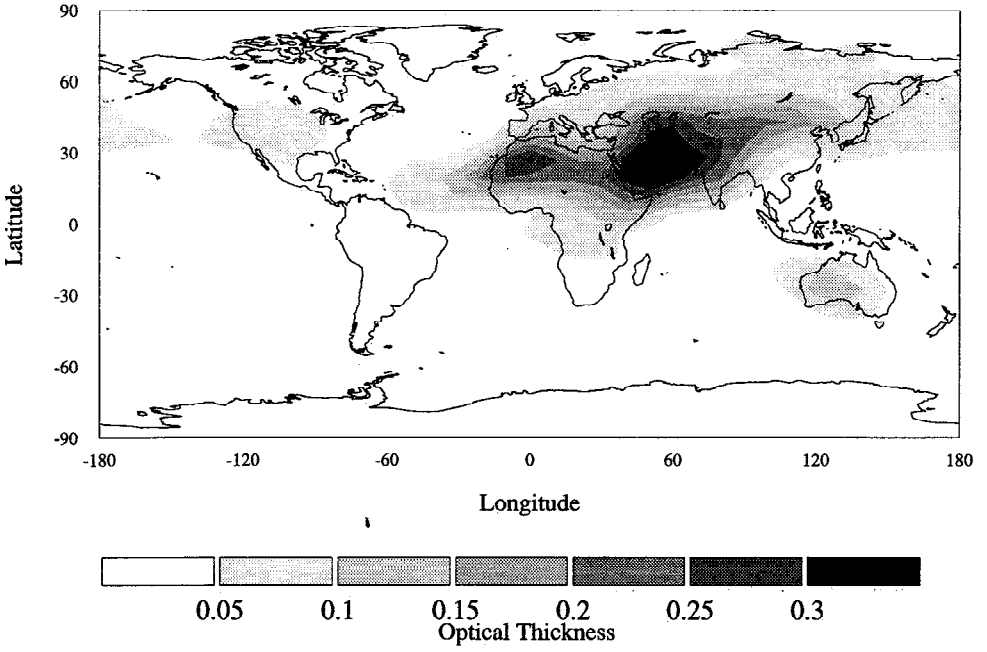

Figure 6. (continued)

6. Conclusions

The results from the model experiments with different source indicate that certain observed seasonal dust distributions can be reproduced only if disturbed sources are taken into account. Furthermore, with the chosen dust source parameterizations the requirements for dust source distributions are fulfilled only if at least 30% of the dust originates from disturbed sources. More likely at least 50% of the dust is of disturbed origin. Even a higher contribution of disturbed dust would be in agreement with the model results. This part of the atmospheric dust load that originates from disturbed soils, can be interpreted as "anthropogenic" dust.

One problem of the dust model experiments is the assumption that dust production in all natural source areas like deserts and sparsely vegetated areas is modeled using the same dependency on surface wind speed and

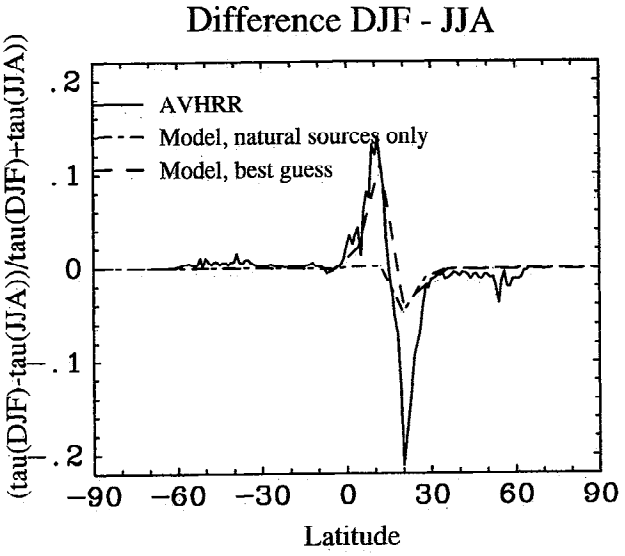

Figure 7. Comparison of the difference in optical thickness between winter and summer months at a latitude of 20°W, as estimated from the AVHRR data product, the model results for only natural sources, and the best guess result (experiment 8 with 50% contribution of dust from disturbed sources).

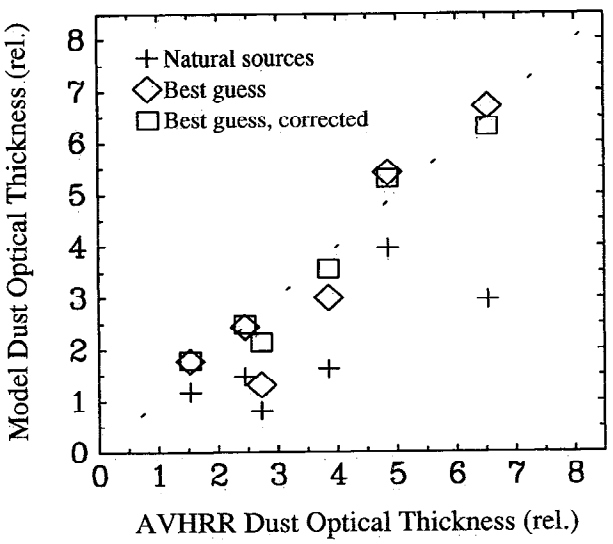

Figure 8. Comparison of the optical thickness ratios (ratios of optical thicknesses at several ocean locations and the optical thickness in the months December–February above the ocean near Australia) of modeled optical thicknesses for the best guess case (with and without correction for biomass burning) and for only natural sources with the AVHRR optical thickness ratios.

soil moisture. In the real world, areas with, say, Wadi sediments or loess deposits, act as stronger sources of dust compared to crusted desert surface. This regional variability was not included in the parameterization of natural dust sources. Also, dust production caused by human activities like road building or military traffic in arid regions was not included in the parameterization of disturbed dust sources. Nevertheless, the calculations give a first-order estimate of contributions from different large-scale dust sources.

The radiative effect of dust is not well known. As it is absorbing in thermal wavelengths and absorbing and reflecting at solar wavelengths, it will supposedly influence atmospheric heating rates in areas with high dust

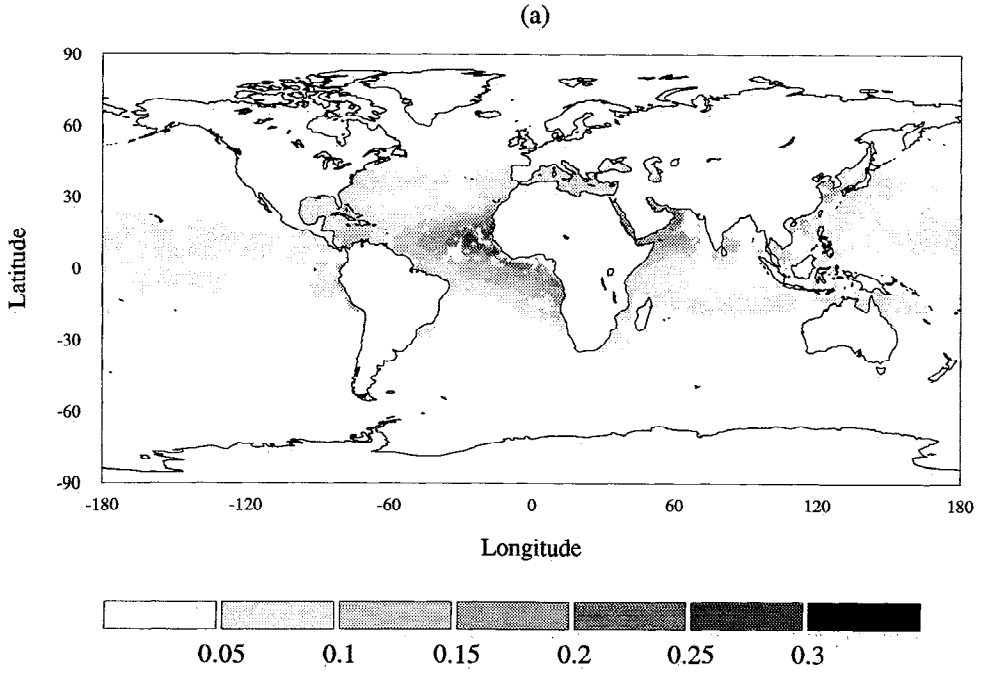

Figure 9. Annual mean optical thickness for (a) the best guess model result, and (b) the annual mean of the AVHRR optical thickness retrievals for the year 1990 [*Ignatov et al.*, 1995; *Rao et al.*, 1988].

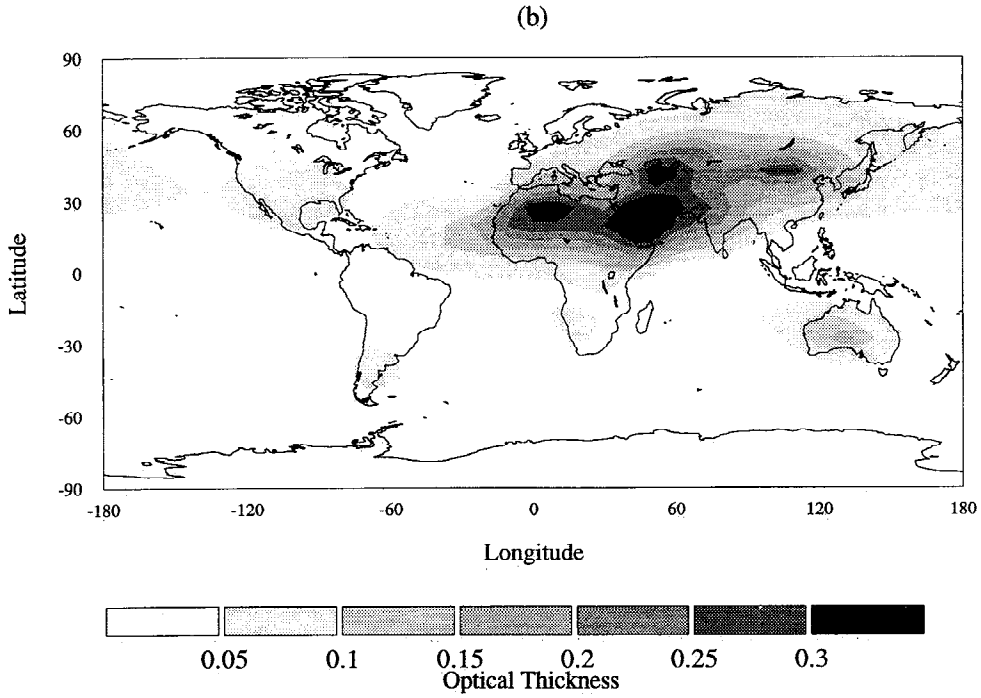

Figure 9. (continued)

loading. If, as our calculations indicate, a large part of the dust load is anthropogenic, this effect needs to be taken into account in estimates of the human impact on the Earth's climate. On the other hand, climate change will in turn influence the dust production. Feedback mechanisms can be anticipated between climate conditions and dust production.

Acknowledgments. This study grew out of a discussion with J. Prospero at the 1994 Dahlem Conference. The support of the NASA Office of the Mission to Planet Earth is acknowledged. This paper is a contribution to the Climate System History and Dynamics Programme that is jointly sponsored by the Natural Sciences and Engineering Research Council of Canada and the Atmospheric Environment Service of Canada.

References

Andreae, M. O., Biomass burning: Its history, use, and distribution and its impact on environmental quality and global climate, in *Global Biomass Burning*, edited by J. S. Levine, pp. 3–21, MIT Press, Cambridge, Mass., 1991.

Andreae, M. O., Climate effects of changing atmospheric aerosol levels, in *World Survey of Climatology, vol. XX, Future Climate of the World*, edited by A. Henderson-Sellers, Elsevier, Amsterdam, in press, 1995.

Bouwman, A. F., I. Fung, E. Matthews, and J. John, Global analysis of the potential for N_2O production in natural soils, *Global Biogeochem. Cycles.*, *7*, 557–579, 1993.

Druyan, L., K.-W. Lo, K. Shah, J. A. Marengo, and G. Russel, Impacts of model improvements on GCM sensitivity to SST forcing., *Int. J. Clim.*, 1994, in press.

Duce, R. A., et al., The atmospheric input of trace species into the world ocean, *Global Biogeochem. Cycles*, *5*, 193–259, 1991.

Fouquart, Y., B. Bonnel, M. Chaoui Roquai, R. Santer, and A. Cerf, Observations of Saharan aerosols: Results of the ECLATS field experiment, 1, optical thickness and aerosol size distribution, *J. Clim. Appl. Meteorol.*, *26*, 28–37, 1987.

Fraser, R. F., Optical thickness of atmospheric dust over Tadzhikistan, *Atmos. Environ.*, *27A*, 2533–2538, 1993.

Fung, I., K. Prentice, E. Matthews, and G. Russell, Three–dimensional tracer model study of atmospheric CO_2: Response to seasonal exchanges with the terrestrial biosphere, *J. Geophys. Res.*, *88*, 1281–1294, 1983.

Fung, I. Y., C. J. Tucker, and K. C. Prentice, Application of Advanced Very High Resolution Radiometer Vegetation Index to study atmosphere–biosphere exchange of CO_2, *J. Geophys. Res.*, *92*, 2999–3015, 1987.

Genthon, C., Simulations of desert dust and sea salt aerosols in Antarctica with a general circulation model of the atmosphere, *Tellus*, *44*, 371–389, 1992.

Gillette, D., A wind tunnel simulation of the erosion of soil: Effect of soil texture, sandblasting, wind speed, and soil consolidation on dust production, *Atmos. Environ.*, *12*, 1735–1743, 1978.

Gillette, D. A., and K. Hanson, Spatial and temporal variability of dust production caused by wind erosion in the United States, *J. Geophys. Res.*, *94*, 2197–2206, 1989.

Gillette, D. A., and P. Sinclair, Estimation of suspension of alkaline material dust devils in the United States, *Atmos. Environ., 24a*, 1135–1142, 1990.

Gillette, D. A., I. H. Blifford, and D. W. Fryrear, The influence of wind velocity on the size distributions of aerosols generated by the wind erosion of soils, *J. Geophys. Res., 79*, 4068–4075, 1974.

Gillette, D. A., J. Adams, A. Endo, D. Smith, and R. Kihl, Threshold velocities for input of soil particles into the air by desert soils, *J. Geophys. Res., 85*, 5621–5630, 1980.

Goudie, A. S., Dust storms in space and time, *Prog. Phys. Geog., 7*, 502–530, 1983.

Ignatov, A. M., L. L. Stowe, S. M. Sakerin, and G. K. Korotaev, Validation of the NOAA NESDIS aerosol satellite product over the north Atlantic in 1989, *J. Geophys. Res., 100*, 5123–5132, 1995.

Jaenicke, R., Aerosol physics and chemistry, in *Landold-Börnstein New Series*, vol. 4, Meteorology, edited by G. Fischer, pp. 391–457, Springer Verlag, New York, 1988.

Joussaume, S., Three-dimensional simulations of the atmospheric cycle of desert dust particles using a general circulation model, *J. Geophys. Res., 95*, 1909–1941, 1990.

Kalma, J. D., J. G. Speight, and R. J. Wasson, Potential wind erosion in Australia: A continental perspective, *J. Clim., 8*, 411–428, 1988.

Lamb, P. J., R. A. Peppler, and S. Hastenrath, Interannual variability in the tropical Atlantic, *Nature, 322*, 238–240, 1986.

Littmann, T., Dust storm frequency in Asia: Climatic control and variability, *Int. J. Clim., 11*, 393–412, 1991.

Matthews, E., New high–resolution data sets for climate studies, *J. Climate Appl. Meteor., 22*, 474–487, 1983.

McDonald, W. F., *Atlas of Climatic Charts of the Oceans*, U.S. Dep. Agric. Weather Bur., Washington, D. C., 1938.

Middelton, N., *World Atlas of Desertification*. Edward Arnold, Kent, 1992.

Oort, A., Global atmospheric circulation statistics 1953–1973, *Tech. Rep., NOAA Prof. Pap. 14*, 1983.

Penner, J. E., R. E. Dickinson, and C. A. O'Neill, Effects of aerosol from biomass burning on the global radiation budget, *Science, 256*, 1432–1433, 1992.

Penner, J. E., R. J. Charlson, J. M. Hales, N. S. Laulainen, R. Leifer, T. Novakov, J. Ogren, L. F. Radke, S. E. Schwartz, and L. Travis, Quantifying and minimizing uncertainty of climate forcing by anthropogenic aerosols, *Bull. Am. Meteorol. Soc., 75*, 375–400, 1994.

Prather, M. J., B. McElroy, S. C. Wofsy, G. R. Russell, and D. Rind, Chemistry of the global troposphere: Fluorocarbons as tracers of air motion, *J. Geophys. Res., 92*, 6579–6613, 1987.

Prospero, J. M., and R. T. Nees, Impact of the North African drought and El Niño on mineral dust in the Barbados trade winds, *Nature, 320*, 735–738, 1986.

Prospero, J. M., R. A. Glaccum, and R. T. Nees, Atmospheric transport of soil dust from Africa to South Amcrica, *Nature, 289*, 570 572, 1981.

Pye, K., *Aeolian Dust and Dust Deposits*, Academic, San Diego, Calif., 1987.

Rao, C. R. N., L. L. Stowe, E. P. McClain, J. Sapper, and M. P. McCormick, Development and application of aerosol remote sensing with AVHRR data from the NOAA satellites, in *Aerosols and Climate*, edited by P. V. hobbs, A. Deepak, Hampton, Va., 1988.

Schütz, L., Long range transport of desert dust with special emphasis on the Sahara, *Ann. N.Y. Acad. Sci., 388*, 515–532, 1980.

Shea, D., Climatological atlas: 1950–1979, surface air temperature, precipitation, sea level pressure, and sea surface temperature, *Tech. Rep., NCAR/TN-269+STR*, Natl. Cent. for Atmos. Res., Boulder, Colo., 1986.

Sirokko, F., and M. Sarntheim, Wind–borne deposits in the northwestern Indian Ocean: Record of Holocene sediments versus modern satellite data, in *Paleoclimatology and Paleometeorology: Modern and Past Patterns of Global Atmospheric Transport*, edited by M. Leinen, and M. Sarntheim, pp. 401–433, Kluwer Academic, Norwll, Mass., 1989.

Tegen, I., and I. Fung, Modeling of mineral dust in the atmosphere: Sources, transport and optical thickness, *J. Geophys. Res., 99*, 22,897–22,914, 1994.

Tucker, C. J., H. E. Dregne, and W. W. Newcomb, Expansion and contraction of the Sahara desert from 1980 to 1990, *Science, 253*, 299–301, 1991.

Webb, R., C. Rosenzweig, and E. R. Levine, A global data set of particle size properties, *Tech. Rep., NASA TM-4286*, 1991.

Wefers, M., and R. Jaenicke, Global 3D distribution of desert aerosols from a numerical simulation, in *Proceedings 3rd International Aerosol Conference, Kyoto, Japan*, edited by S. Masuda, and K. Takakashi, pp. 1086–1089, 1990.

Westphal, D. L., A two–dimesional numerical investigation of the dynamics and microphysics of Saharan dust storms, *J. Geophys. Res., 92*, 3027–3049, 1987.

World Resources Institute, *World Resources 1992-1993*, edited by A. L. Hammond. Oxford University Press, New York, 1992.

Zobler, L., A world file for global climate modeling, *Tech. Rep., NASA-TM-87802*, 1986.

Inez Fung, School of Earth and Ocean Sciences, University of Victoria, P.O. Box 1700, Victoria, British Columbia, V8W 2Y2, Canada, (e-mail: inez@garryoak.seaoar.uvic.ca)

Ina Tegen, Department of Applied Physics, Columbia University, 2880 Broadway, New York, NY 10025. (e-mail: cxixt@giss.nasa.gov)

(Received December 26, 1994; revised May 15, 1995; accepted May 15, 1995.)